

Quantum parameter estimation with optimal control

Jing Liu and Haidong Yuan*

*Department of Mechanical and Automation Engineering,
The Chinese University of Hong Kong, Shatin, Hong Kong*

A pivotal task in quantum metrology, and quantum parameter estimation in general, is to design schemes that achieve the highest precision with given resources. Standard models of quantum metrology usually assume the dynamics is fixed, the highest precision is achieved by preparing the optimal probe states and performing optimal measurements. However, in many practical experimental settings, additional controls are usually available to alter the dynamics. Here we propose to use optimal control methods for further improvement on the precision limit of quantum parameter estimation. We show that by exploring the additional degree of freedom offered by the controls higher precision limit can be achieved. In particular we show that the precision limit under the controlled schemes can go beyond the constraints put by the coherent time, which is in contrast to the standard scheme where the precision limit is always bounded by the coherent time.

PACS numbers: 03.67.-a, 03.65.Yz, 03.65.-w.

I. INTRODUCTION

Quantum metrology, which exploits quantum mechanical effects to achieve high precision, has gained increased attention in recent years [1–25]. A typical metrological procedure is to first encode the interested parameter x on a probe state ρ_0 via a parameter dependent dynamics \mathcal{E}_x , i.e., $\rho_0 \xrightarrow{\mathcal{E}_x} \rho_x$, then perform a set of Positive Operator Valued Measurements (POVM) on ρ_x . Based on the measurement results an estimation \hat{x} can then be obtained. It is known that for unbiased estimation quantum Cramér-Rao bound sets a lower bound on the precision [26–29] $\delta\hat{x} \geq 1/\sqrt{F}$, where $\delta\hat{x}$ is the standard deviation and F is the quantum Fisher information (QFI). If the procedure is repeated n times, then $\delta\hat{x} \geq 1/\sqrt{nF}$ where the bound can be achieved in the asymptotical limit.

In this standard procedure, the dynamics \mathcal{E}_x is usually assumed to be fixed, and the highest precision is achieved by preparing the optimal probe state and performing the optimal POVM that saturates the quantum Cramér-Rao bound. The obtained precision is often regarded as the ultimate precision. However, in many experimental settings, additional controls are usually available to alter the dynamics for further improvement of the precision limit, this provides another degree of freedom for optimization.

The parallel scheme and the sequential scheme, as shown in Fig. 1, are two standard schemes considered in quantum parameter estimation. It is known that if the dynamics is unitary and the Hamiltonian takes the multiplication form of the parameter, i.e., if $\mathcal{E}_x = e^{-ixH}$, then the two schemes are equivalent [30]; while for general unitary dynamics $\mathcal{E}_x = e^{-iH(x)}$, the parallel scheme is equivalent to the controlled sequential scheme [17]. For noisy quantum parameter estimation, special controlled schemes, such as quantum error correction and dynamical decoupling, have been used to improve the precision

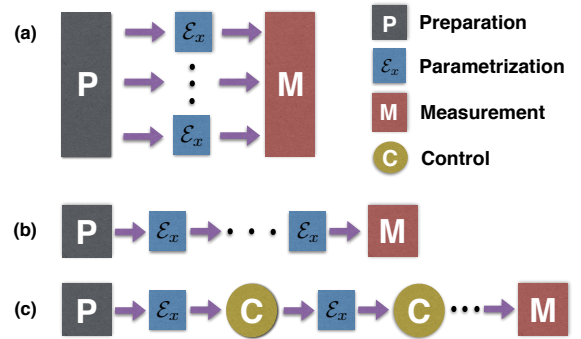


Figure 1. (Color online) (a) Parallel scheme; (b) Sequential scheme; (c) Controlled sequential scheme.

limit [31–40]. The controlled sequential scheme is more implementable on current experimental settings than the parallel scheme, as high-fidelity controls on small systems can now be routinely done while preparing large entangled states for the parallel scheme is still very challenging. The controlled sequential scheme thus starts to gain attention recently [36–41]. Existing controlled schemes that use quantum error correction or dynamical decoupling either need additional resources such as auxiliary systems that are completely immune to noises or require the underlying dynamics possessing certain symmetries, which restrict the scope of the applications. Systematic methods that can design controls to improve the precision limit for general dynamics are highly desired in practice.

In this paper we propose to employ optimal quantum control methods, in particular the Gradient Ascent Pulse Engineering (GRAPE) [42], to design controls for the improvement of the precision limit in quantum parameter estimation. Such methods can be used to automatically obtain the optimal controls for the improvement of the precision limit for general dynamics and can easily incorporate practical constraints on the controls. It thus provides a general method to design the controlled schemes in quantum metrology. With this method we

* hdyuan@mae.cuhk.edu.hk

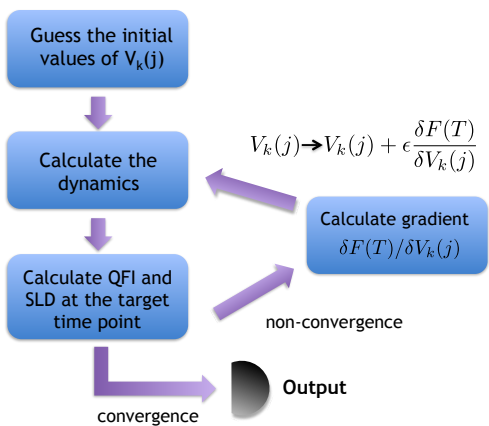


Figure 2. (Color online) The flow chart of the algorithm. The key for this algorithm is to update the controls based on the gradient value.

will show that the optimally controlled schemes can obtain precision limits beyond the coherent time, which is in contrast to the conventional schemes where the precision limit is always bounded by the coherent time.

II. METHODOLOGY

In this article we consider the system whose dynamics can be described by the master equation

$$\partial_t \rho(t) = \mathcal{L}[\rho(t)], \quad (1)$$

where \mathcal{L} is a super-operator. For unitary evolution $\mathcal{L} = -iH^\times$ where $H^\times(\rho) = [H, \rho]$; for noisy evolution $\mathcal{L} = -iH^\times + \Gamma$ where Γ denotes the super-operator for the noisy process. The Hamiltonian of a controlled system can be written as [42, 44]

$$H = H_0(x) + \sum_{k=1}^p V_k(t) H_k, \quad (2)$$

where $H_0(x)$ is the free evolution Hamiltonian, x is the interested parameter, $\sum_{k=1}^p V_k(t) H_k$ are control Hamiltonians with $V_k(t)$ representing the amplitude of k th control field. Here we assume the correlation in the environment decays much faster than the evolution of the system under Eq. (1), and the Markovian approximation is still valid at the presence of controls [43]. For example, in Nuclear Magnetic Resonance, the correlation time of the environment is around 10^{-6} s and the coherent time is around $0.1 \sim 1$ s [44], if the time scale of the control is around 10^{-3} s, then the Markovian approximation is valid, and the controls are fast enough to generate the desired operations. We also assume the controls do not change the noisy operators, this holds under some physical settings [45–47] but not in general. The situations that noisy operators are affected by controls will be addressed in another work.

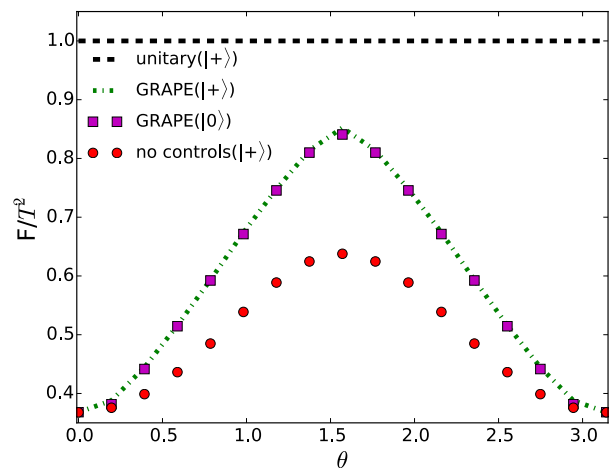


Figure 3. (Color online) The QFI (normalized by T^2) as a function of θ . The dash-dotted green line, purple squares and circled red dots represent the QFI with and without controls, respectively. The dashed black line represent the value of QFI for unitary evolution. The target time $T = 5$, and decay rate $\gamma = 0.1$. The states in the bracket in the legend represent the corresponding initial state. The true values of ω_0 is assumed to be 1.

To implement the GRAPE we will divide the evolution time T into small time steps, and within each time step Δt the controls will be approximated as constants. The final state at time T can thus be written as $\rho(T) = \Pi_{i=1}^m \exp(\Delta t \mathcal{L}_i) \rho(0)$, here $m = T/\Delta t$ is the number of time steps and \mathcal{L}_i is the super-operator for the i th time step. The multiplication in $\rho(T)$ is taken from right to left.

GRAPE can obtain controls that optimize a given objective function. In this article we focus on the local precision limit for the measurement of small shifts around certain known values. Such local precision limit can be quantified by the QFI, we will thus take the QFI as the objective function. The QFI is defined as

$$F(T) = \text{Tr} [\rho(T) L_s^2(T)], \quad (3)$$

where $L_s(T)$ denotes the symmetric logarithmic derivative (SLD) which is the solution to the equation $\partial_x \rho(T) = [\rho(T) L_s(T) + L_s(T) \rho(T)] / 2$. The flow of the algorithm is shown in Fig. 2 (detailed description is in appendix A). Some steps of the algorithm may require the knowledge of x , which is a-priori unknown, in that case an estimated value \hat{x} will be used and the controls will be updated adaptively. This, however, does not affect the precision limit asymptotically.

In practical experiments, the measurements that can be taken are restricted. It is thus also of practical importance to find the optimal controls that can lead to the highest precision under a fixed measurement, which is quantified by the classical Fisher information (CFI) F_{cl} under the particular measurement, instead of the QFI. This can also be treated via GRAPE. Given a set of

POVM measurement $\{E(y)\}$ with $\sum_y E(y) = \mathbf{1}$, the probability of getting the measurement result y is given by $p_{y|x} = \text{Tr}(\rho(T)E(y))$, and the CFI is given by

$$F_{\text{cl}}(T) = \sum_y \frac{(\partial_x p_{y|x})^2}{p_{y|x}}. \quad (4)$$

III. APPLICATION

We first apply the algorithm to the phase estimation with a two-level system under dephasing dynamics. The dynamics is given by [43]

$$\partial_t \rho = -i[H, \rho] + \frac{\gamma}{2} (\sigma_{\vec{n}} \rho \sigma_{\vec{n}} - \rho), \quad (5)$$

here the system Hamiltonian is $H = \frac{1}{2}\omega_0\sigma_3 + \vec{V}(t) \cdot \vec{\sigma}$ with $\vec{V}(t) = (V_1(t), V_2(t), V_3(t))$, $\vec{\sigma} = (\sigma_1, \sigma_2, \sigma_3)$. σ_1, σ_2 and σ_3 are Pauli matrices. The dephasing is along $\sigma_{\vec{n}} = \vec{n} \cdot \vec{\sigma}$ with $\vec{n} = (\sin\theta \cos\phi, \sin\theta \sin\phi, \cos\theta)$. Here $\theta \in [0, \pi]$, $\phi \in [0, 2\pi]$. ω_0 is the parameter to be estimated. Here we assume the controls can be performed along all three directions, however the results hold as long as the controls span $\mathfrak{su}(2)$.

In Fig. 3 we plotted the QFIs with different dephasing dynamics for $T = 5$ (the unit is taken in the order of ω_0^{-1}). The different dephasing dynamics are characterized by the angle θ (ϕ is taken as zero, as we can always make a rotation along σ_3 direction to make ϕ equal to zero and such rotation does not affect the precision). From the figure we can see that the highest enhancement, compared to the uncontrolled schemes, occurs at $\theta = \pi/2$ where the noise is transverse to the direction of the parameter, and the enhancement reduces when θ goes to zero (parallel noises). We note that here no ancillary systems are used, which is different from previous studies using quantum error correction where ancillary systems are necessary [36–40]. Besides, in this case, the highest precision does not strongly depend on the probe state, which can be seen in Fig. 3. $|0\rangle$ (purple squares) and $|+\rangle = (|0\rangle + |1\rangle)/\sqrt{2}$ (dash-dotted green line) provide almost the same precision under the optimal controlled scheme.

We next provide some analysis on the controlled scheme under different noises to give some physical intuitions on how the controls actually helped improving the precision limit.

A. Transverse dephasing

The improvement of the controlled scheme with transverse noises is shown in Fig. 4(a). When the probe state is taken as $|+\rangle$, the obtained optimal controls are $V_1(t) = V_2(t) = 0$ and $V_3(t) = -0.5\omega_0$, shown in Fig. 4(b). Such controls essentially keep the probe state

at $|+\rangle$, where it is not affected by the noises. The QFI under such controls is given by (see appendix for detailed derivation)

$$F(T) = \frac{2}{\gamma^2} (e^{-\gamma T} + \gamma T - 1). \quad (6)$$

It always increases with T as $F'(T) > 0$. The precision limit thus is not constrained by the coherent time. In contrast, without controls there is an optimal time T_{opt} (which is determined by the decay rate, for example when $\omega_0 \gg \gamma$, $T_{\text{opt}} \simeq 2/\gamma$), at which the precision reaches the maximum, and beyond T_{opt} the QFI starts to decrease with time, which can be seen in Fig. 4(a).

We note in this case the control $V_3(t) = -0.5\omega_0$ depends on the true value which is a-priori unknown, in practice an estimated value $\hat{\omega}_0$ need to be used and the controls need to be updated adaptively according to the estimated value as $V_3(t) = -0.5\hat{\omega}_0$. In Fig. 4(c) we plotted the improvement provided by the controls with different estimation error, it can be seen that the improvement is quite robust. For example assume the true value $\omega_0 = 1$ and $T = 20$, then as long as $\hat{\omega}_0 \in [0.8, 1.2]$ the controlled scheme outperforms the uncontrolled scheme, and when $\hat{\omega}_0 \in [0.9, 1.1]$, the QFI under the controlled scheme is more than 10 times larger than the value without controls, thus even with a 10% estimation error the controlled scheme still provides significant improvement over the uncontrolled schemes.

If the measurement is fixed, for example the measurement is taken as $\{|+\rangle\langle+|, |-\rangle\langle-|\}$ (here $|\pm\rangle = (|0\rangle \pm |1\rangle)/\sqrt{2}$), we can also use the optimal control to improve the precision. From Fig. 4(a) we can see that with the optimal controls the CFI can actually achieve the maximal QFI, indicating that the precision limit under the optimal controlled scheme is insensitive to the measurement performed on the final state, as long as it is projective. This is because the optimal measurement (which is a projective measurement) can always be rotated to the fixed measurement which corresponds to a counter rotation on the probe state that can be achieved via controls. As a comparison the precision without controls is also plotted, in this case the CFI oscillate with time and can only reach the QFI for some specific time points, indicating this measurement scheme is only optimal for some specific time points. From Fig. 4(c) it can be seen that the precision obtained is also very robust against the estimation error.

B. Parallel dephasing

We now provide some analysis for the case with parallel dephasing, which is usually a more dominant noise for many physical systems [49, 50], and cannot be corrected by quantum error correction techniques even with ancillary systems [36–40].

The QFI under parallel dephasing are shown in Fig. 5(a). It can be seen that the QFI under optimal

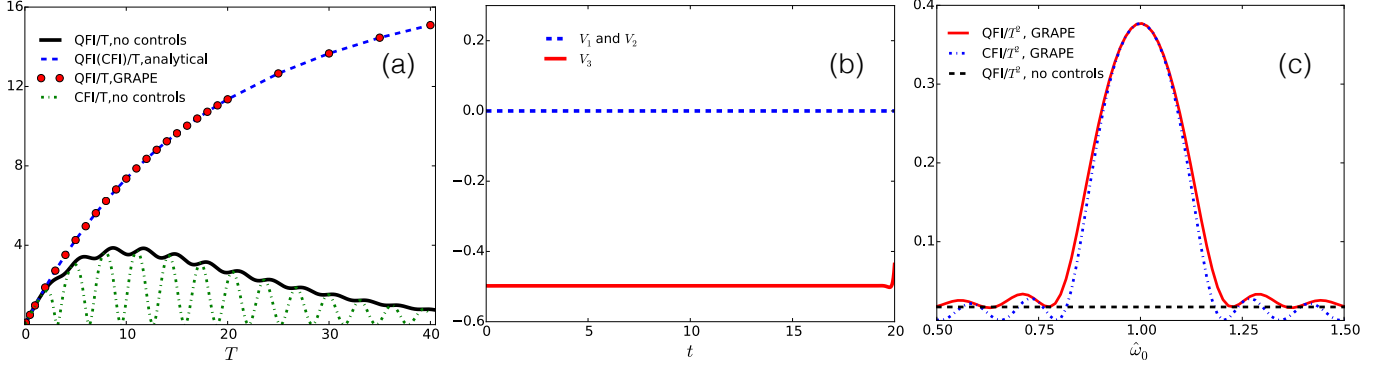


Figure 4. (Color online) Transverse dephasing: (a) The evolution of QFI (normalized by T) with and without controls. The red dots and black lines represent the QFI with and without controls, respectively (the wiggles in the black line is not numerical error but caused by some trigonometric functions in the QFI in this case). The dashed blue line is the analytical solution for the QFI (and CFI) under controls. The dash-dotted green line is the CFI without controls. Decay rate $\gamma = 0.1$, and the measurement for CFI is $\{|+\rangle\langle+|, |-\rangle\langle-|\}$. (b) Optimal controls obtained from the GRAPE. (c) The enhanced QFI and CFI (normalized by T^2) as a function of $\hat{\omega}_0$. The solid red and dash-dotted blue lines represent the QFI and CFI under controls, respectively. The target time $T = 20$ and $\gamma = 0.2$. The dashed black line represents the value of QFI without controls. The true values of ω_0 in all panels are assumed to be 1.

control continues to increase beyond the coherent time, while in contrast the QFI without control starts to decrease beyond the coherent time.

To gain some intuition on how controls improved the precision we consider a simple control strategy: we first prepare the probe state as $|+\rangle$ and let it evolve under the natural evolution (without controls) for a period of t_0 , then apply a $\pi/2$ -pulse along y -direction, after that let the state evolve for another period of $T - t_0$ under the natural evolution. To analyze the effect of this strategy we write the state with the Bloch representation as $\rho = (\mathbb{1} + \vec{r} \cdot \vec{\sigma})/2$, the initial state $|+\rangle$ thus corresponds to $(r_1(0), r_2(0), r_3(0)) = (1, 0, 0)$. Under the free evolution the state evolves as

$$r_1(t) = e^{-\gamma t} [\sin(\omega_0 t) r_2(0) + \cos(\omega_0 t) r_1(0)], \quad (7)$$

$$r_2(t) = e^{-\gamma t} [\cos(\omega_0 t) r_2(0) - \sin(\omega_0 t) r_1(0)], \quad (8)$$

$$r_3(t) = r_3(0), \quad (9)$$

which gives $\vec{r}(t) = e^{-\gamma t} (\cos(\omega_0 t), -\sin(\omega_0 t), 0)$. If no controls are added, the QFI for ω_0 can be easily computed using the following formula [51]

$$F(t) = |\partial_{\omega_0} \vec{r}(t)|^2 + \frac{(\vec{r}(t) \cdot \partial_{\omega_0} \vec{r}(t))^2}{1 - |\vec{r}(t)|^2}, \quad (10)$$

which gives $F(t) = t^2 e^{-2\gamma t}$, the maximum is achieved at the coherent time $T_{\text{opt}} = 1/\gamma$.

Now assume the target time is T and we perform the rotation

$$R_y = \begin{pmatrix} 0 & 0 & -1 \\ 0 & -1 & 0 \\ 1 & 0 & 0 \end{pmatrix} \quad (11)$$

at some time point $t_0 < T$. The quantum state after the R_y -rotation is $e^{-\gamma t_0} (0, \sin(\omega_0 t_0), \cos(\omega_0 t_0))$, which, after

another free evolution with a period of $\Delta t = T - t_0$, leads to the final state $\vec{r}(T) = (r_1(T), r_2(T), r_3(T))$ where

$$r_1(T) = e^{-\gamma T} \sin(\omega_0 \Delta t) \sin(\omega_0 t_0), \quad (12)$$

$$r_2(T) = e^{-\gamma T} \cos(\omega_0 \Delta t) \sin(\omega_0 t_0), \quad (13)$$

$$r_3(T) = e^{-\gamma t_0} \cos(\omega_0 t_0). \quad (14)$$

The QFI can again be calculated from Eq. (10), with t_0 as a variable that can be changed to maximize $F(T)$ (the explicit form of $F(T)$ is in the appendix).

Figure 5(b) shows the QFI as a function of t_0 , one can see that for $T = 5$, no matter when the rotation is performed, the QFI cannot be higher than the QFI without rotations. However, for $T = 15$, as long as the rotation is performed at a proper time point, we can obtain an improved QFI. It can also be seen that the QFI usually has multiple peaks with the variation of t_0 , the maximum peak may differ for different T . The maximum QFI thus may not be smooth with respect to T .

In Fig. 5(a) we plotted the maximum QFI that can be achieved with this simple control strategy. It can be seen that this strategy does not help improving the QFI when T is smaller than some time T^* (which is approximately the coherent time $\gamma^{-1} = 10$ in this case, same behaviour are found for other values of γ), however when T gets big, a control pulse at a proper time t_0 improves the QFI. The intuition of this simple strategy is that although states in the x - y plane have a fast rate of parametrization under the Hamiltonian $\omega_0 \sigma_3$, they are also affected most by the parallel noise, when T gets large the effect of noise overrides the parametrization, applying pulses at proper time that rotate the states away from x - y plane help mitigate the noise effect thus improve the precision. More rotations can further improve the precision and GRAPE essentially provides a systematical way to find these rotations.

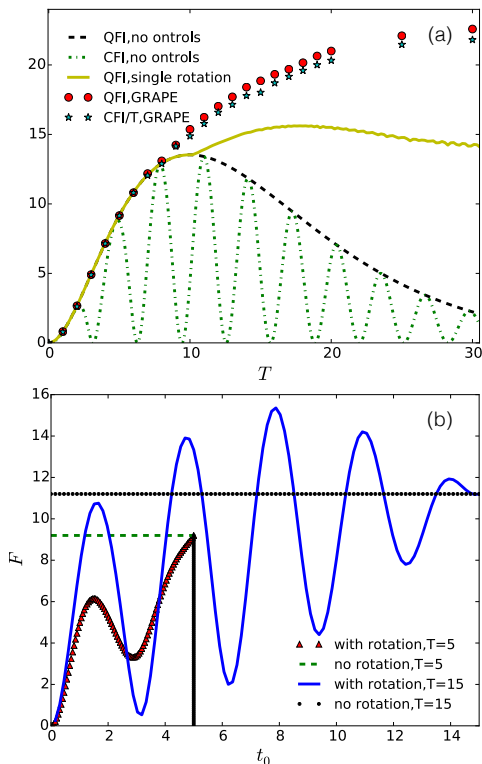


Figure 5. (Color online) Parallel dephasing: (a) The evolution of QFI with and without controls. The red dots and solid black lines represent the QFI with and without controls, respectively. The solid yellow line represent the maximum QFI with single $\pi/2$ pulse along y -axis at a proper time. The green stars and dash-dotted green lines represent the CFI with and without controls, respectively. The measurement for CFI is $\{|+\rangle\langle +|, |-\rangle\langle -|\}$ (b) QFI as a function of t_0 . The solid blue and triangular red lines represent the QFI with rotation at t_0 , for $T = 15$ and $T = 5$, respectively. The dotted black and dashed green lines represent the QFIs without rotation.

This is contrary to the conventional belief that coherent time sets the limit on the achievable precision, which is particular useful for those systems where the preparation of the probe states and the measurements are costly and one would like to extract more information for each measurement. Note that for the local precision limit which measures small shifts around certain known value, the phase can still be distinguished even under a long evolution time. For completely unknown phase, one needs to first evolve for a short time to avoid the possible ambiguity as the phase may wrap around the 2π interval. However after a rough estimation, the evolution time can get longer.

If the cost for the preparation and measurement is negligible, we should compare the QFI per unit of time, which is called the normalized QFI. As shown in Fig 6(a), with controls the maximum value of the normalized QFI is not improved compared to the values without controls (dashed black line), which indicates the normalized precision limit is still bounded by the coherent time

under the parallel dephasing. However, when a fixed measurement is considered, for example the projective measurement $\{|+\rangle\langle +|, |-\rangle\langle -|\}$, the advantage of control shows up. With optimal controls the CFI is very close to the maximum QFI, indicating that the measurement $\{|+\rangle\langle +|, |-\rangle\langle -|\}$ is almost optimal under the controlled scheme, while without controls the CFI oscillates with time and is usually far from the maximum QFI.

In Fig. 6(b), the optimal controls obtained from the GRAPE are plotted. Generally the optimal control is not unique and the appearance of the controls in Fig. 6(b) is due to the algorithm. Such kind of controls seem complicated, but have been routinely implemented on physical systems, such as Nuclear Magnetic Resonance [52–56]. Various techniques have also been developed to smooth the controls [57, 58]. And as shown in Fig. 6(c) the controls obtained are again quite robust against the estimation error (in this figure we first obtain the controls with $\hat{\omega}_0 = 1$, then apply the controls to dynamics with different ω_0). It can be seen that the controlled scheme gains over the uncontrolled scheme with a quite broad range ($\sim 10\%$) of estimation error.

C. Spontaneous emission

We give some analysis for the controlled scheme at the presence of the spontaneous emission, which is another major noise for many practical systems. We consider the general master equation

$$\begin{aligned} \partial_t \rho(t) = & -i[H, \rho] + \gamma_+ \left[\sigma_+ \rho(t) \sigma_- - \frac{1}{2} \{ \sigma_- \sigma_+, \rho(t) \} \right] \\ & + \gamma_- \left[\sigma_- \rho(t) \sigma_+ - \frac{1}{2} \{ \sigma_+ \sigma_-, \rho(t) \} \right], \end{aligned} \quad (15)$$

where $\sigma_{\pm} = (\sigma_1 \pm i\sigma_2)/2$ is a ladder operator, $H = \frac{1}{2}\omega_0\sigma_3 + \vec{V}(t) \cdot \vec{\sigma}$.

The effects of the controls are shown in Figure 7(a). In this case the normalized QFI under the controlled scheme shows significant improvement over the value without controls. And similar to the dephasing case, under the measurement $\{|+\rangle\langle +|, |-\rangle\langle -|\}$, the normalized CFI (dashed blue line) not only achieves the maximum value, but also ceases to oscillate.

Again we use a simple control strategy with only one rotation to provide some intuition on how controls helped improving the precision. For simplicity, we assume $\gamma_+ = 0$ and $\gamma_- = \gamma$. In the Bloch representation, without the controls the states evolves as

$$r_1(t) = e^{-\frac{1}{2}\gamma t} [\cos(\omega_0 t) r_1(0) - \sin(\omega_0 t) r_2(0)], \quad (16)$$

$$r_2(t) = e^{-\frac{1}{2}\gamma t} [\cos(\omega_0 t) r_2(0) + \sin(\omega_0 t) r_1(0)], \quad (17)$$

$$r_3(t) = -1 + e^{-\gamma t} + e^{-\gamma t} r_3(0). \quad (18)$$

If the initial state is taken as $|+\rangle$, then the QFI at time t is $F = e^{-\gamma t} t^2$ and the maximum is achieved at $T_{\text{opt}} = 2/\gamma$.

Now consider a simple control strategy: we first let the initial state, which is $|+\rangle$, evolve for some time t_0 under

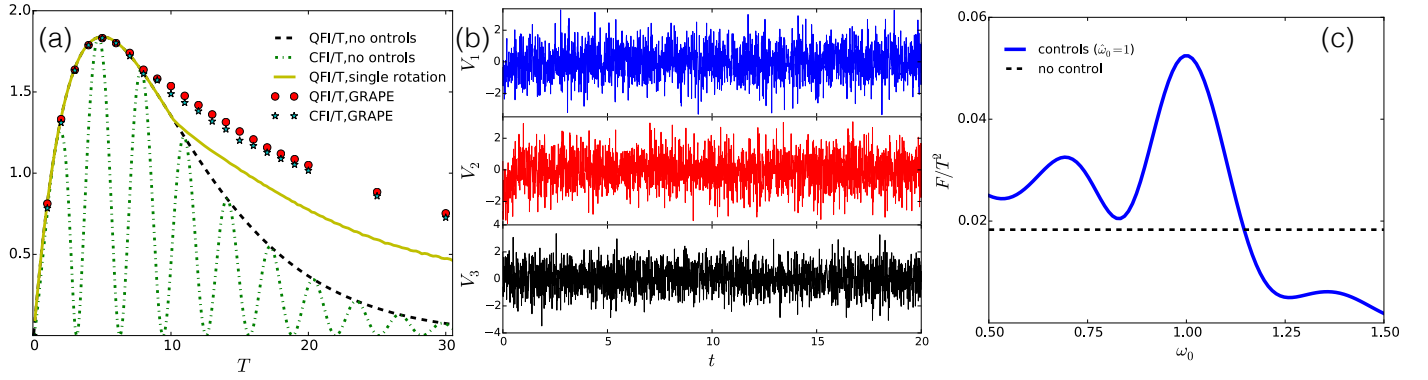


Figure 6. (Color online) Parallel dephasing: (a) The evolution of normalized QFI (by T) with and without controls. The red dots and solid black line represent the normalized QFI with and without controls, respectively. The solid yellow line represent the maximum normalized QFI with single $\pi/2$ pulse along y -axis at a proper time. The green stars and dash-dotted green lines represent the normalized CFI with and without controls, respectively. The measurement for CFI is $\{|+\rangle\langle +|, |-\rangle\langle -|\}$ (b) The controls obtained from GRAPE for the dynamics with $T = 20$. The initial guessing is randomly. (c) The normalized QFI (by T^2) for different ω_0 . the controls are obtained from the GRAPE for $\omega_0 = 1$. It can be seen that the QFI of the controlled scheme is higher than the QFI of the uncontrolled scheme as long as $|\omega_0 - 1|$ is not too big, i.e., as long as the estimated value is reasonably good. The true values of ω_0 are assumed to be 1 and decay rate $\gamma = 0.1$ in all panels.

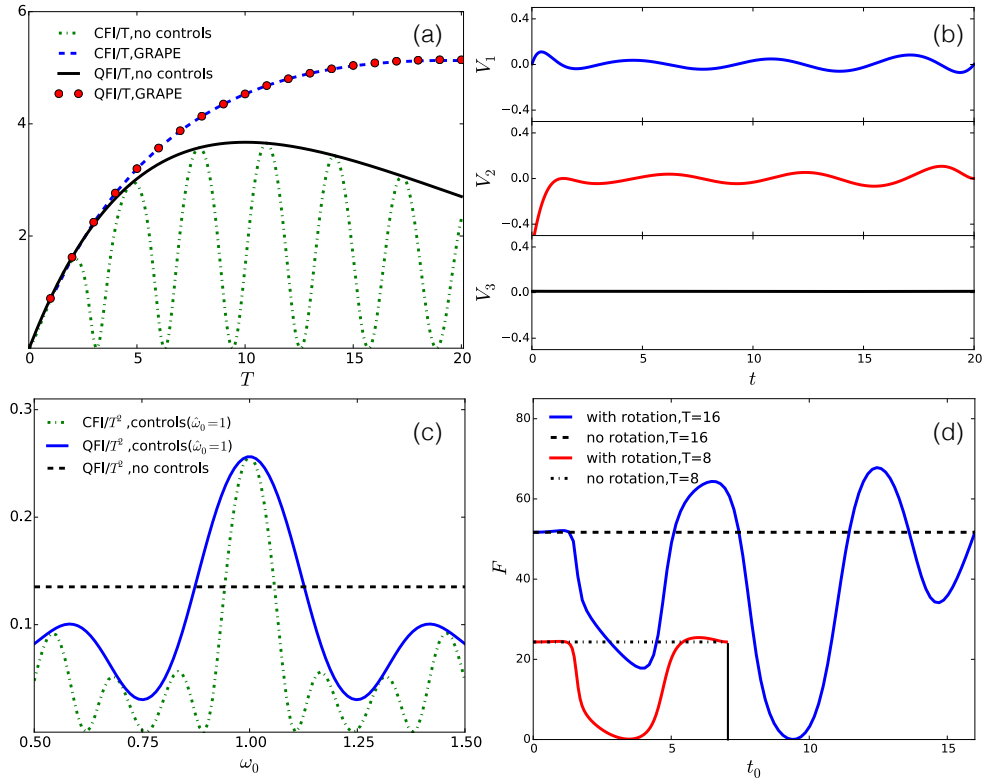


Figure 7. (Color online) Spontaneous emission: (a) normalized QFI (by T) as a function of T . The red dots and solid black lines represent the QFI with and without controls, respectively. And the dashed blue and dash-dotted green lines represent the CFI with and without controls, respectively. Here $\gamma_+ = 0$, $\gamma_- = 0.1$. The true value of ω_0 is 1. The measurement for CFI is $\{|+\rangle\langle +|, |-\rangle\langle -|\}$. (b) The controls obtained from GRAPE for the dynamics with $T = 20$. The initial guessing is all zero. (c) The QFI and CFI (normalized by T^2) as a function of ω_0 . The solid blue and dash-dotted green lines represent the QFI and CFI under the controls given by GRPAE with $\hat{\omega}_0 = 1$, respectively. The dashed black line is the QFI without controls. (d) QFI as a function of t_0 . The solid blue and red lines represent the QFI with rotation at t_0 , for $T = 16$ and $T = 8$, respectively. The dashed and dash-dotted black lines represent the QFIs without rotation.

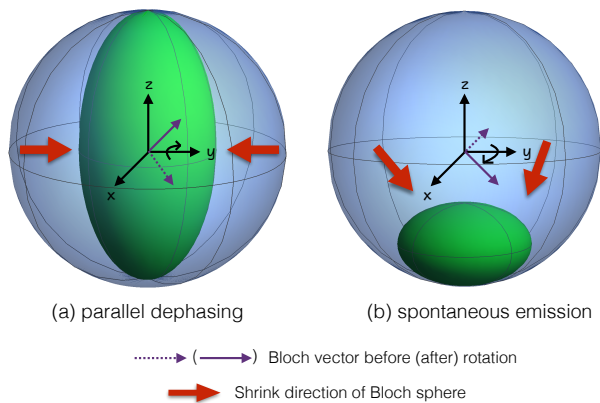


Figure 8. (Color online) Schematic for the effects of parallel dephasing and spontaneous emission on the Bloch sphere. The blue spheres and green spheres represent the initial and evolved state space in the noise.

the free evolution (in this case the free evolution will drive the state away from the $x-y$ plane of the Bloch sphere), we then apply a control to rotate the state back to the $x-y$ plane, let it evolve for another period, $T-t_0$. The derivation of the QFI under this simple control strategy is given in appendix F.

In Fig. 7(d), we plotted the QFI under this simple control strategy as a function of t_0 for $T=8, 16$. Here the control strategy is different from the parallel dephasing case. Under the parallel dephasing (the effects of the parallel dephasing on the states are shown in Fig. 8(a)), the states in the $x-y$ plane are affected most by the dephasing noise although they also undergo the fastest parametrization. For a long evolution time, the dephasing noise can override the parametrization, thus applying a control rotating the state away from $x-y$ plane is beneficial under the parallel dephasing. While under the spontaneous emission (with the effect on the states shown in Fig. 8(b)), the initial state is in the $x-y$ plane, which has the fastest parameterizations, but the free evolution quickly drives the states away from the $x-y$ plane before the noises override the parametrization. It is thus beneficial to apply a control rotating the state back to the $x-y$ plane for a fast parametrization. Also for the spontaneous emission the states in the $x-y$ plane are not the states affected most by the noise.

D. Energy cost

We provide some estimation on the energy cost for the optimal controls implemented in some of the examples. In Fig. 9 we plot the energy cost $E(t) = \sum_k \int_0^t V_k^2(\tau) d\tau$ of the optimal controls as a function of time within the total time $T=10$. It can be seen that for the examples, the implementations of optimal controls do not require much energy and thus it will not be an obstacle in practice. Note that in the case of the parallel dephasing, there is

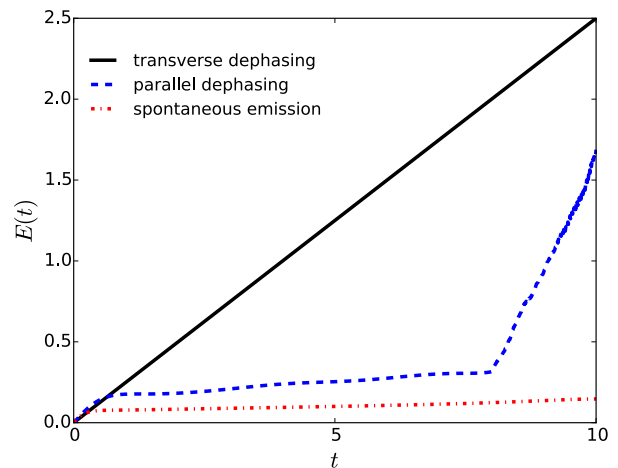


Figure 9. (Color online) The energy cost $E(t)$ (in the scale of $\omega_0 = 1$) for performing the controls in the case of transverse dephasing (solid black line), parallel dephasing (dashed blue line) and spontaneous emission (dash-dotted red line) with the target time $T=10$. The decay rates in all cases are 0.1.

a sudden change near the coherent time. This is due to the fact that under the parallel dephasing controls do not have much effect far before the coherent time, therefore it needs little controls in this regime. Strong controls only starts to appear near the coherent time.

IV. SUMMARY

For many current experimental settings the controlled sequential scheme is more implementable than the parallel scheme since high-fidelity controls can now be routinely done on many physical systems, such as nuclear magnetic resonance [52–56], nitrogen-vacancy centers [59–61] and cold atoms [62]. GRAPE provides a general method to obtain optimal controls for the improvement of the precision limit, which is expected to find wide applications for many practical quantum parameter estimation tasks.

As a demonstration we applied the method to the frequency estimation with different noises and showed that GRAPE can improve the precision limit beyond the limit set by the coherent time, which is contrary to the conventional belief that coherent time sets the limit on the achievable precision. This is particular useful for those systems where the measurements are costly and one would like to extract more information for each measurement. For the dephasing cases, we showed that the gain of the controlled scheme is most eminent when the dephasing noise is orthogonal to the Hamiltonian, while when the noise is parallel to the Hamiltonian, the controls do not increase the precision one can obtain per unit of time. Future research includes characterizing the dynamics and noises for which the controls are (un)useful.

The optimal control method can also be used for non-

Markovian dynamics [63–65] and easily incorporate various practical constraints on pulse shape [57, 58, 66–68], thus provides a versatile tool for designing controlled schemes for various quantum parameter estimation tasks.

ACKNOWLEDGMENTS

H. Yuan acknowledges partial financial support from RGC of Hong Kong with Grant No. 538213.

Appendix A: Algorithm description

GRAPE can obtain controls that optimize a given objective function. In this article we focus on the local precision limit for the measurement of small shifts around certain known values. Such local precision limit can be quantified by the QFI, we will thus take the QFI as the objective function. The QFI is given by $F(T) = \text{Tr}[\rho(T)L_s^2(T)]$ where $L_s(T)$ denotes the symmetric logarithmic derivative (SLD) which is the solution to the equation $\partial_x \rho(T) = [\rho(T)L_s(T) + L_s(T)\rho(T)]/2$. The flow of the algorithm is as following:

1. guess initial values of $V_k(j)$ (here $V_k(j)$ denotes the k th control at the j th time step);
2. evolve the dynamics and obtain a trajectory of the system;
3. calculate the QFI at the target time;
4. calculate the gradient $\frac{\delta F(T)}{\delta V_k(j)}$;
5. update $V_k(j)$ to $V_k(j) + \epsilon \frac{\delta F(T)}{\delta V_k(j)}$;
6. restart from step 2 using the updated $V_k(j)$ until the QFI converges.

The detailed calculation of $\frac{\delta F(T)}{\delta V_k(j)}$ is in appendix B. The gradient of the QFI can be written as

$$\frac{\delta F(T)}{\delta V_k(j)} = \Delta t \text{Tr} \left[L_s^2(T) \mathcal{M}_j^{(1)} \right] - 2\Delta^2 t \text{Tr} \left[L_s(T) \left(\mathcal{M}_j^{(2)} + \mathcal{M}_j^{(3)} \right) \right], \quad (\text{A1})$$

where $\mathcal{M}_j^{(1)}$, $\mathcal{M}_j^{(2)}$ and $\mathcal{M}_j^{(3)}$ are Hermitian operators and in the form below

$$\begin{aligned} \mathcal{M}_j^{(1)} &= i \mathcal{D}_{j+1}^m H_k^\times (\rho_j), \\ \mathcal{M}_j^{(2)} &= \sum_{i=1}^j \mathcal{D}_{j+1}^m H_k^\times \mathcal{D}_{i+1}^j \dot{H}_0^\times (\rho_i), \\ \mathcal{M}_j^{(3)} &= (1 - \delta_{jm}) \sum_{i=j+1}^m \mathcal{D}_{i+1}^m \dot{H}_0^\times \mathcal{D}_{j+1}^i H_k^\times (\rho_j), \end{aligned} \quad (\text{A2})$$

here δ_{jm} is Kronecker delta function. $L_s(T)$ is the SLD of $\rho(T)$, $\mathcal{D}_{j+1}^m := \prod_{i=j+1}^m \exp(\Delta t \mathcal{L}_i)$ is the propagating

superoperator from the j th time point to the target time, $j < m$ (we will let $\mathcal{D}_i^i = \mathbb{1}$ when $i > i'$). $\rho_j = \mathcal{D}_1^j \rho(0)$ is the state at the j th time point. $H_k^\times = [H_k, \cdot]$ and $\dot{H}_0^\times = [\partial_x H_0, \cdot]$.

In practical experiments, the measurements that can be taken are restricted. It is thus also of practical importance to find the optimal controls that can lead to the highest precision under a fixed measurement, which is quantified by the CFI F_{cl} under the particular measurement, instead of the QFI. This can also be treated via GRAPE. Given a set of POVM measurement $\{E(y)\}$ with $\sum_y E(y) = \mathbb{1}$, the probability of getting the measurement result y is given by $p_{y|x} = \text{Tr}(\rho(T)E(y))$, and the CFI is given by $F_{\text{cl}}(T) = \sum_y \frac{(\partial_x p_{y|x})^2}{p_{y|x}}$. The gradient of F_{cl} can be similarly obtained as Eq. (A1), which is

$$\frac{\delta F_{\text{cl}}(T)}{\delta V_k(j)} = \Delta t \text{Tr} \left(\tilde{L}_2 \mathcal{M}_j^{(1)} \right) - 2\Delta^2 t \text{Tr} \left[\tilde{L}_1 \left(\mathcal{M}_j^{(2)} + \mathcal{M}_j^{(3)} \right) \right], \quad (\text{A3})$$

where

$$\tilde{L}_1 = \sum_y (\partial_x \ln p_y) E(y), \quad (\text{A4})$$

$$\tilde{L}_2 = \sum_y (\partial_x \ln p_y)^2 E(y). \quad (\text{A5})$$

Here $\mathcal{M}_j^{(1,2,3)}$ takes the same form as in Eq. (A2) (see appendix C for detailed derivation).

Appendix B: Gradient for QFI

The dynamics for the density matrix of a system can be described by the following general master equation

$$\partial_t \rho(t) = \mathcal{L}[\rho(t)], \quad (\text{B1})$$

where \mathcal{L} is a super-operator and $\mathcal{L} = -iH^\times + \Gamma$. $H^\times = [H, \cdot]$ and Γ is the super-operator for the noise part. The Hamiltonian here is

$$H = H_0(x) + \sum_{k=1}^p V_k(t) H_k, \quad (\text{B2})$$

where $H_0(x)$ is the free evolution Hamiltonian, x is the interested parameter, $\sum_{k=1}^p V_k(t) H_k$ are control Hamiltonians with $V_k(t)$ representing the amplitude of k th control field.

Our objective function is the QFI and the goal is to find the optimal control to obtain the maximum QFI. The QFI is defined as

$$F(T) = \text{Tr}(L_s^2(T)\rho(T)), \quad (\text{B3})$$

where $L_s(T)$ is the SLD operator at target time T and is determined by the equation $2\partial_x \rho(T) = \rho(T)L_s(T) + L_s(T)\rho(T)$.

Before utilizing GRAPE to obtain the optimal control, it is necessary to know the corresponding gradient for QFI on the control coefficients, i.e., $\frac{\delta F(T)}{\delta V_k(j)}$ based on the general master equation. In this section we will show the detailed calculation for the general dynamics given by Eq. (B1).

Since $F(T) = \text{Tr} [L_s^2(T) D_{j+1}^m \rho_j] = \text{Tr} [\lambda_j \rho_j]$, here $L_s(T)$ is the symmetric logarithm derivative of $\rho(T)$, $D_{j+1}^m := \prod_{i=j+1}^m \exp(\Delta t \mathcal{L}_i)$ is the propagating superoperator from the j th time point to the target time, $j < m$ (we will let $D_i^i = \mathbf{1}$ when $i > i'$), $\rho_j = D_1^j \rho(0)$ is the state at the j th time point and $\lambda_j = L_s^2(T) D_{j+1}^m$. The gradient of the QFI with respect to the controls at the j th time step $\frac{\delta F(T)}{\delta V_k(j)}$ can then be computed

$$\frac{\delta F(T)}{\delta V_k(j)} = \text{Tr} \left(\frac{\delta \lambda_j}{\delta V_k(j)} \rho_j \right) + \text{Tr} \left(\lambda_j \frac{\delta \rho_j}{\delta V_k(j)} \right). \quad (\text{B4})$$

we calculate both terms in the following.

1) First we calculate $\delta \rho_j / \delta V_k(j)$. Here the only term contains $V_k(j)$ is the propagator at the j th time point, $e^{\Delta t \mathcal{L}_j}$. Since $\rho_j = e^{\Delta t \mathcal{L}_j} \rho_{j-1}$, we have

$$\frac{\delta \rho_j}{\delta V_k(j)} = \frac{\delta e^{\Delta t \mathcal{L}_j}}{\delta V_k(j)} \rho_{j-1}. \quad (\text{B5})$$

It is known that the derivative of an exponential operator is $\partial_x e^{A(x)} = \int_0^1 e^{sA} (\partial_x A) e^{(1-s)A} ds$. Thus,

$$\frac{\delta e^{\Delta t \mathcal{L}_j}}{\delta V_k(j)} = \int_0^1 e^{\tau \Delta t \mathcal{L}_j} \left(\Delta t \frac{\delta \mathcal{L}_j}{\delta V_k(j)} \right) e^{-\tau \Delta t \mathcal{L}_j} d\tau e^{\Delta t \mathcal{L}_j}. \quad (\text{B6})$$

Since $\mathcal{L}_j(\cdot) = -i[H_0 + \sum_k V_k(j) H_k, \cdot] + \Gamma(\cdot)$, we have $\frac{\delta \mathcal{L}_j}{\delta V_k(j)} = -i H_k^\times$, where H_k^\times represents the commutation superoperator, i.e., $H_k^\times A = [H_k, A]$. We thus have

$$\frac{\delta e^{\Delta t \mathcal{L}_j}}{\delta V_k(j)} = -i \Delta t \int_0^1 e^{\tau \Delta t \mathcal{L}_j} H_k^\times e^{-\tau \Delta t \mathcal{L}_j} d\tau e^{\Delta t \mathcal{L}_j}, \quad (\text{B7})$$

which can be rewritten as

$$\frac{\delta e^{\Delta t \mathcal{L}_j}}{\delta V_k(j)} = -i \Delta t \int_0^1 e^{\tau \Delta t \mathcal{L}_j^\times} H_k^\times d\tau e^{\Delta t \mathcal{L}_j}. \quad (\text{B8})$$

Expand it with the Taylor series,

$$\begin{aligned} \frac{\delta e^{\Delta t \mathcal{L}_j}}{\delta V_k(j)} &= -i \Delta t \int_0^1 \sum_{n=0}^{\infty} \frac{(\tau \Delta t)^n}{n!} d\tau (\mathcal{L}_j^\times)^n H_k^\times e^{\Delta t \mathcal{L}_j} \\ &= -i \sum_{n=0}^{\infty} \frac{(\Delta t)^{n+1}}{(n+1)!} (\mathcal{L}_j^\times)^n H_k^\times e^{\Delta t \mathcal{L}_j} \\ &= -i \Delta t H_k^\times e^{\Delta t \mathcal{L}_j}, \end{aligned} \quad (\text{B9})$$

where the last equation we used the first order approximation. Thus

$$\frac{\delta \rho_j}{\delta V_k(j)} = -i \Delta t H_k^\times \rho_j. \quad (\text{B10})$$

2) Next we calculate $\text{Tr}[\rho_j \delta \lambda_j / \delta V_k(j)]$. We first consider the cases when $j < m$. Since $\lambda_j = L_s^2(T) D_{j+1}^m$, and D_{j+1}^m does not contain $V_k(j)$, thus $\frac{\delta \lambda_j}{\delta V_k(j)} = \frac{\delta L_s^2(T)}{\delta V_k(j)} D_{j+1}^m$, we then have

$$\begin{aligned} \text{Tr} \left(\frac{\delta \lambda_j}{\delta V_k(j)} \rho_j \right) &= \text{Tr} \left(\frac{\delta L_s(T)}{\delta V_k(j)} L_s(T) \rho(T) \right) \\ &\quad + \text{Tr} \left(L_s(T) \frac{\delta L_s(T)}{\delta V_k(j)} \rho(T) \right). \end{aligned} \quad (\text{B11})$$

where we used the fact that $D_{j+1}^m \rho_j = \rho(T)$.

Now take the functional derivative at both sides of the equation $\partial_x \rho(T) = [\rho(T) L_s(T) + L_s(T) \rho(T)]/2$, then multiply $L_s(T)$ and take the trace, we get

$$\begin{aligned} &\text{Tr} \left[\frac{\delta (\partial_x \rho(T))}{\delta V_k(j)} L_s(T) \right] \\ &= \text{Tr} \left[\frac{\delta \rho(T)}{\delta V_k(j)} L_s^2(T) \right] + \frac{1}{2} \text{Tr} \left[\rho(T) \frac{\delta L_s(T)}{\delta V_k(j)} L_s(T) \right] \\ &\quad + \frac{1}{2} \text{Tr} \left[\frac{\delta L_s(T)}{\delta V_k(j)} \rho(T) L_s(T) \right]. \end{aligned} \quad (\text{B12})$$

Compare with Eq. (B11), we then have

$$\begin{aligned} &\text{Tr} \left[\frac{\delta (\partial_x \rho(T))}{\delta V_k(j)} L_s(T) \right] \\ &= \text{Tr} \left[\frac{\delta \rho(T)}{\delta V_k(j)} L_s^2(T) \right] + \frac{1}{2} \text{Tr} \left(\frac{\delta \lambda_j}{\delta V_k(j)} \rho_j \right), \end{aligned} \quad (\text{B13})$$

which means

$$\begin{aligned} &\text{Tr} \left(\frac{\delta \lambda_j}{\delta V_k(j)} \rho_j \right) \\ &= 2 \text{Tr} \left[\frac{\delta (\partial_x \rho(T))}{\delta V_k(j)} L_s(T) \right] - 2 \text{Tr} \left[\frac{\delta \rho(T)}{\delta V_k(j)} L_s^2(T) \right]. \end{aligned} \quad (\text{B14})$$

Since $\text{Tr} \left[\frac{\delta \rho(T)}{\delta V_k(j)} L_s^2(T) \right] = \text{Tr} \left[L_s^2(T) D_{j+1}^m \frac{\delta \rho_j}{\delta V_k(j)} \right] = \text{Tr} \left(\lambda_j \frac{\delta \rho_j}{\delta V_k(j)} \right)$, we thus have

$$\begin{aligned} &\text{Tr} \left(\frac{\delta \lambda_j}{\delta V_k(j)} \rho_j \right) \\ &= 2 \text{Tr} \left[\left(\frac{\delta (\partial_x \rho(T))}{\delta V_k(j)} \right) L_s(T) \right] - 2 \text{Tr} \left(\lambda_j \frac{\delta \rho_j}{\delta V_k(j)} \right) \\ &= 2 \text{Tr} \left[\partial_x \left(\frac{\delta \rho(T)}{\delta V_k(j)} \right) L_s(T) \right] - 2 \text{Tr} \left(\lambda_j \frac{\delta \rho_j}{\delta V_k(j)} \right), \end{aligned} \quad (\text{B15})$$

where the last equality we assume the functional derivative and partial differentiation can be exchanged. Substitute Eq. (B15) into Eq. (B4), we can obtain the expression for the gradient, which is

$$\frac{\delta F(T)}{\delta V_k(j)} = 2 \text{Tr} \left[\partial_x \left(\frac{\delta \rho(T)}{\delta V_k(j)} \right) L_s(T) \right] + i \Delta t \text{Tr} \left(\lambda_j H_k^\times \rho_j \right). \quad (\text{B16})$$

We now derive $\partial_x \left(\frac{\delta \rho(T)}{\delta V_k(j)} \right)$. Since $\frac{\delta \rho(T)}{\delta V_k(j)} = \mathcal{D}_{j+1}^m \frac{\delta \rho_j}{\delta V_k(j)}$, we have

$$\begin{aligned} \partial_x \left(\frac{\delta \rho(T)}{\delta V_k(j)} \right) &= \Delta t \sum_{i=j+1}^m \mathcal{D}_{i+1}^m (\partial_x \mathcal{L}_i) \mathcal{D}_{j+1}^i \frac{\delta \rho_j}{\delta V_k(j)} \\ &\quad + \mathcal{D}_{j+1}^m \partial_x \left(\frac{\delta \rho_j}{\delta V_k(j)} \right), \end{aligned} \quad (\text{B17})$$

where in the first term we used the fact that in the first order

$$\partial_x e^{\Delta t \mathcal{L}_i} = \Delta t (\partial_x \mathcal{L}_i) e^{\Delta t \mathcal{L}_i} \quad (\text{B18})$$

From Eq. (B10), we then have $\partial_x \left(\frac{\delta \rho_j}{\delta V_k(j)} \right) = \partial_x (-i \Delta t H_k^\times \rho_j) = -i \Delta t H_k^\times \partial_x \rho_j$. Now as

$$\begin{aligned} \partial_x \rho_j &= \Delta t \sum_{i=1}^j \mathcal{D}_{i+1}^j (\partial_x \mathcal{L}_i) \mathcal{D}_1^i \rho_0 \\ &= \Delta t \sum_{i=1}^j \mathcal{D}_{i+1}^j (\partial_x \mathcal{L}_i) \rho_i, \end{aligned} \quad (\text{B19})$$

one have $\partial_x \left(\frac{\delta \rho_j}{\delta V_k(j)} \right) = -i \Delta^2 t \sum_{i=1}^j H_k^\times \mathcal{D}_{i+1}^j (\partial_x \mathcal{L}_i) \rho_i$. With this expression, we have

$$\mathcal{D}_{j+1}^m \partial_x \left(\frac{\delta \rho_j}{\delta V_k(j)} \right) = -i \Delta^2 t \sum_{i=1}^j \mathcal{D}_{j+1}^m H_k^\times \mathcal{D}_{i+1}^j (\partial_x \mathcal{L}_i) \rho_i.$$

Thus

$$\begin{aligned} \partial_x \left(\frac{\delta \rho(T)}{\delta V_k(j)} \right) &= -i \Delta^2 t \sum_{i=j+1}^m \mathcal{D}_{i+1}^m (\partial_x \mathcal{L}_i) \mathcal{D}_{j+1}^i H_k^\times \rho_j \\ &\quad - i \Delta^2 t \sum_{i=1}^j \mathcal{D}_{j+1}^m H_k^\times \mathcal{D}_{i+1}^j (\partial_x \mathcal{L}_i) \rho_i. \end{aligned} \quad (\text{B20})$$

Note that here we cannot discard $\Delta^2 t$ as the second order, as we have a summation which can effectively add up to cancel one order of Δt (for example $\Delta^2 t \sum_{i=1}^m 1 = m \Delta^2 t = T \Delta t$).

Furthermore, as $\mathcal{L}_i(\cdot) = -i [H_0 + \sum_k V_k(i) H_k, \cdot] + \Gamma(\cdot)$, and only the free Hamiltonian H_0 contains x , we have $\partial_x \mathcal{L}_i = -i [\partial_x H_0, \cdot] = -i (\partial_x H_0)^\times$. Thus, Eq. (B20) can be expressed by

$$\begin{aligned} \partial_x \left(\frac{\delta \rho(T)}{\delta V_k(j)} \right) &= -\Delta^2 t \sum_{i=j+1}^m \mathcal{D}_{i+1}^m (\partial_x H_0)^\times \mathcal{D}_{j+1}^i H_k^\times \rho_j \\ &\quad - \Delta^2 t \sum_{i=1}^j \mathcal{D}_{j+1}^m H_k^\times \mathcal{D}_{i+1}^j (\partial_x H_0)^\times \rho_i \end{aligned} \quad (\text{B21})$$

Multiplying $L_s(T)$ on both sides of the equation above

and taking the trace gives

$$\begin{aligned} &\text{Tr} \left[\partial_x \left(\frac{\delta \rho(T)}{\delta V_k(j)} \right) L_s(T) \right] \\ &= -\Delta^2 t \sum_{i=j+1}^m \text{Tr} \left[L_s(T) \mathcal{D}_{i+1}^m (\partial_x H_0)^\times \mathcal{D}_{j+1}^i H_k^\times \rho_j \right] \\ &\quad - \Delta^2 t \sum_{i=1}^j \text{Tr} \left[L_s(T) \mathcal{D}_{j+1}^m H_k^\times \mathcal{D}_{i+1}^j (\partial_x H_0)^\times \rho_i \right]. \end{aligned} \quad (\text{B22})$$

Utilizing above equation, one can obtain the final expression for the gradient, which is

$$\begin{aligned} \frac{\delta F(T)}{\delta V_k(j)} &= -2 \Delta^2 t \sum_{i=j+1}^m \text{Tr} \left[L_s(T) \mathcal{D}_{i+1}^m (\partial_x H_0)^\times \mathcal{D}_{j+1}^i H_k^\times \rho_j \right] \\ &\quad - 2 \Delta^2 t \sum_{i=1}^j \text{Tr} \left[L_s(T) \mathcal{D}_{j+1}^m H_k^\times \mathcal{D}_{i+1}^j (\partial_x H_0)^\times \rho_i \right] \\ &\quad + i \Delta t \text{Tr} \left[L_s^2(T) \mathcal{D}_{j+1}^m H_k^\times \rho_j \right]. \end{aligned} \quad (\text{B23})$$

For the case when $j = m$, the gradient is $\frac{\delta F(T)}{\delta V_k(m)} = 2 \text{Tr} \left[\left(\partial_x \frac{\delta \rho_m}{\delta V_k(m)} \right) L_s(T) \right] + i \text{Tr} \left[L_s^2(T) \Delta t H_k^\times \rho_m \right]$. In this case, $\delta \rho_m / \delta V_k(m) = -i \Delta t H_k^\times \rho_m$, thus

$$\begin{aligned} &\text{Tr} \left[\left(\partial_x \frac{\delta \rho_m}{\delta V_k(m)} \right) L_s(T) \right] \\ &= -\Delta^2 t \sum_{i=1}^m \text{Tr} \left[L_s(T) H_k^\times \mathcal{D}_{i+1}^m (\partial_x H_0)^\times \rho_i \right]. \end{aligned} \quad (\text{B24})$$

the gradient is then

$$\begin{aligned} \frac{\delta F(T)}{\delta V_k(m)} &= -2 \Delta^2 t \sum_{i=1}^m \text{Tr} \left[L_s(T) H_k^\times \mathcal{D}_{i+1}^m (\partial_x H_0)^\times \rho_i \right] \\ &\quad + i \Delta t \text{Tr} \left[L_s^2(T) H_k^\times \rho_m \right]. \end{aligned} \quad (\text{B25})$$

Combine this equation with Eq. (B23), the gradient of the QFI can be written compactly as the from in the main text.

Appendix C: Gradient for CFI

It is known that CFI is

$$F_{\text{cl}}(T) = \sum_y \frac{(\partial_\theta p_y)^2}{p_y}, \quad (\text{C1})$$

where $p_y = \text{Tr}(\rho(x, T) E(y))$. Here $E(y)$ is a POVM measurement which satisfying $\sum_y E(y) = \mathbb{1}$. To calculate the gradient, we need to know

$$\begin{aligned} \frac{\delta p_y}{\delta V_k(j)} &= \text{Tr} \left[\frac{\delta \rho(T)}{\delta V_k(j)} E(y) \right] \\ &= \text{Tr} \left[\mathcal{D}_{j+1}^m \frac{\delta \rho_j}{\delta V_k(j)} E(y) \right] \\ &= -i \Delta t \text{Tr} \left[E(y) \mathcal{D}_{j+1}^m H_k^\times \rho_j \right] \\ &= -\Delta t \text{Tr} \left[E(y) \mathcal{M}_j^{(1)} \right]. \end{aligned} \quad (\text{C2})$$

Then we have

$$\begin{aligned} \frac{\delta(\partial_x p_y)}{\delta V_k(j)} &= -i\Delta t \text{Tr} [E(y) \partial_x (D_{j+1}^m H_k^\times \rho_j)] \\ &= -i\Delta t \text{Tr} \left\{ E(y) \left[(\partial_x D_{j+1}^m) H_k^\times \rho_j \right. \right. \\ &\quad \left. \left. + D_{j+1}^m H_k^\times \partial_x \rho_j \right] \right\}. \end{aligned} \quad (\text{C3})$$

From previous calculations, we know

$$\partial_x D_{j+1}^m = \Delta t \sum_{i=j+1}^m D_{i+1}^m (\partial_x \mathcal{L}_i) D_{j+1}^i, \quad (\text{C4})$$

$$\partial_x \rho_j = \Delta t \sum_{i=1}^j D_{i+1}^j (\partial_x \mathcal{L}_i) \rho_i, \quad (\text{C5})$$

then for $j \neq m$,

$$\begin{aligned} \frac{\delta(\partial_x p_y)}{\delta V_k(j)} &= -\Delta^2 t \text{Tr} \left[\left(E(y) \sum_{i=j+1}^m D_{i+1}^m \dot{H}_0^\times D_{j+1}^i H_k^\times \rho_j \right. \right. \\ &\quad \left. \left. + \sum_{i=1}^j D_{j+1}^m H_k^\times D_{i+1}^j \dot{H}_0^\times \rho_i \right) \right]. \end{aligned} \quad (\text{C6})$$

for $j = m$, there is

$$\begin{aligned} \frac{\delta(\partial_x p_y)}{\delta V_k(m)} &= -i\Delta t \text{Tr} [E(y) H_k^\times \partial_x \rho_m] \\ &= -\Delta^2 t \text{Tr} \left[E(y) H_k^\times \sum_{i=1}^m D_{i+1}^j \dot{H}_0^\times \rho_i \right]. \end{aligned}$$

Thus, combined above equations, we have

$$\frac{\delta(\partial_x p_y)}{\delta V_k(j)} = -\Delta^2 t \text{Tr} \left\{ E(y) \left[\mathcal{M}_j^{(2)} + \mathcal{M}_j^{(3)} \right] \right\}.$$

Finally, the gradient is

$$\begin{aligned} \frac{\delta F_{\text{cl}}(T)}{\delta V_k(j)} &= \sum_y \frac{\delta}{\delta V_k(j)} \left(\frac{(\partial_x p_y)^2}{p_{\text{T}}(y|x)} \right) \\ &= \sum_y 2 \frac{\partial_x p_y}{p_y} \left[\frac{\delta(\partial_x p_y)}{\delta V_k(j)} \right] - \left(\frac{\partial_x p_y}{p_y} \right)^2 \frac{\delta p_y}{\delta V_k(j)} \\ &= \sum_y -2\Delta^2 t \frac{\partial_x p_y}{p_y} \text{Tr} \left[E(y) \left(\mathcal{M}_j^{(2)} + \mathcal{M}_j^{(3)} \right) \right] \\ &\quad + \Delta t \left(\frac{\partial_x p_y}{p_y} \right)^2 \text{Tr} \left(E(y) \mathcal{M}_j^{(1)} \right). \end{aligned} \quad (\text{C7})$$

The gradient for CFI is then obtained.

Appendix D: Analytical solution for transverse dephasing noise

For the dynamics with transverse dephasing noises, the controls obtained from the GRAPE are shown in Fig. 4(b), which are $V_x = 0$, $V_y = 0$ and $V_z = -\omega_0/2$.

The QFI under such control is the same as the QFI under free evolution for $\omega_0 = 0$, which can actually be computed analytically. In the following we give a detailed calculation.

Under the Bloch representation $\rho = \frac{1}{2} (\mathbb{1} + \vec{r} \cdot \vec{\sigma})$, the initial state $|+\rangle$ can be expressed as $\vec{r}(0) = (1, 0, 0)$. From the master equation we can obtain the differential equations for the Bloch vector as

$$\partial_t r_1(t) = \omega_0 r_2(t), \quad (\text{D1})$$

$$\partial_t r_2(t) = -\gamma r_2(t) - \omega_0 r_1(t), \quad (\text{D2})$$

$$\partial_t r_3(t) = -\gamma r_3(t). \quad (\text{D3})$$

The solution of these equations are

$$r_1(t) = e^{-\frac{1}{2}\gamma t} \left[\frac{\gamma}{a} \sinh\left(\frac{1}{2}at\right) + \cosh\left(\frac{1}{2}at\right) \right], \quad (\text{D4})$$

$$r_2(t) = -\frac{2\omega_0}{a} e^{-\frac{1}{2}\gamma t} \sinh\left(\frac{1}{2}at\right), \quad (\text{D5})$$

$$r_3(t) = 0, \quad (\text{D6})$$

where $a = \sqrt{\gamma^2 - 4\omega_0^2}$. We will now compute $f(\rho_{\omega_0}, \rho_{\omega_0 + \delta\omega_0})$ where $f(\rho_1, \rho_2) = \text{Tr} \sqrt{\sqrt{\rho_1} \rho_2 \sqrt{\rho_1}}$ denotes the fidelity, the QFI can then be obtained from the second order expansion of $f(\rho_{\omega_0}, \rho_{\omega_0 + \delta\omega_0})$ for $\omega_0 = 0$. It is easy to see that $\vec{r}(t)|_{\omega_0=0} = (1, 0, 0)$, which is $|+\rangle = \frac{1}{\sqrt{2}}(|0\rangle + |1\rangle)$ and the fidelity between $|+\rangle$ and an evolved state with a general ω_0 is

$$f = \sqrt{\langle + | \frac{1}{2} (\mathbb{1} + \vec{r}(t) \cdot \vec{\sigma}) | + \rangle} = \sqrt{\frac{1}{2} + \frac{1}{2} r_1(t)}. \quad (\text{D7})$$

For a small $\delta\omega_0$, up to the second order we have $a = \gamma - \frac{2}{\gamma} \delta^2 \omega_0$ and $\frac{\gamma}{a} = 1 + \frac{2}{\gamma^2} \delta^2 \omega_0$, then

$$\begin{aligned} r_1(t) &= e^{-\frac{1}{2}\gamma t} \left[\frac{\gamma}{a} \sinh\left(\frac{1}{2}at\right) + \cosh\left(\frac{1}{2}at\right) \right] \\ &= e^{-\frac{t}{\gamma} \delta^2 \omega_0} + \frac{2}{\gamma^2} \delta^2 \omega_0 \frac{e^{-\frac{t}{\gamma} \delta^2 \omega_0} - e^{-\gamma t} e^{\frac{t}{\gamma} \delta^2 \omega_0}}{2} \\ &= 1 - \frac{1}{\gamma^2} (e^{-\gamma t} + \gamma t - 1) \delta^2 \omega_0. \end{aligned} \quad (\text{D8})$$

Thus the fidelity is

$$\begin{aligned} f(\rho_0, \rho_{\delta\omega_0}) &= \sqrt{1 - \frac{1}{2} \frac{1}{\gamma^2} (e^{-\gamma t} + \gamma t - 1) \delta^2 \omega_0} \\ &= 1 - \frac{1}{4} \frac{1}{\gamma^2} (e^{-\gamma t} + \gamma t - 1) \delta^2 \omega_0. \end{aligned} \quad (\text{D9})$$

The QFI can then be obtained from the second order term as

$$F(t) = \frac{2}{\gamma^2} (e^{-\gamma t} + \gamma t - 1). \quad (\text{D10})$$

Now we consider the classical Fisher information under optimal controls. Taking the measurement as $\{|+\rangle\langle +|, |-\rangle\langle -|\}$, then the probabilities are $p_+(t) = (1 +$

$r_1(t)/2$ and $p_- = (1 - r_1(t))/2$. The corresponding classical Fisher information is

$$F_{\text{class}}(t) = \frac{(\partial_{\omega_0} p_+)^2}{p_+ p_-} = \frac{(\partial_{\omega_0} r_1)^2}{1 - r_1^2(t)}. \quad (\text{D11})$$

For the the controls $\hat{\omega}_0 \sigma_3/2$, where $\hat{\omega}_0$ is very close to ω_0 , based on Eq. (D8), one can see $1 - r_1^2(t) = F(t) \delta^2 \omega_0$ and $\partial_{\omega_0} r_1(t) = -F(t) \delta \omega_0$, which indicates $F_{\text{class}}(t) = F(t)$, i.e., the measurement $\{|+\rangle\langle+|, |-\rangle\langle-|\}$ is the optimal measurement to access the quantum Fisher information.

Appendix E: Parallel dephasing

Here we consider the simple control strategy for the dynamics with parallel dephasing noises. Recall that the strategy is to first prepare the probe state at $|+\rangle$ and let it evolve under the natural evolution (without controls) for a period of t_0 , then apply a $\pi/2$ -pulse along y -direction and let it evolve for another period of $T - t_0$. As shown in the main text the final state at T in the Bloch representation is given by $\vec{r}(T) = (r_1(T), r_2(T), r_3(T))$ with

$$r_1(T) = e^{-\gamma T} \sin(\omega_0 \Delta t) \sin(\omega_0 t_0), \quad (\text{E1})$$

$$r_2(T) = e^{-\gamma T} \cos(\omega_0 \Delta t) \sin(\omega_0 t_0), \quad (\text{E2})$$

$$r_3(T) = e^{-\gamma t_0} \cos(\omega_0 t_0), \quad (\text{E3})$$

from which we can obtain the QFI using the following formula [51]

$$F(T) = |\partial_{\omega_0} \vec{r}(T)|^2 + \frac{(\vec{r}(T) \cdot \partial_{\omega_0} \vec{r}(T))^2}{1 - |\vec{r}(T)|^2}, \quad (\text{E4})$$

specifically,

$$\begin{aligned} F(T) &= e^{-2\gamma t_0} t_0^2 \sin^2(\omega_0 t_0) \\ &\quad + e^{-2\gamma T} [t_0^2 + T(T - 2t_0) \sin^2(\omega_0 t_0)] \\ &\quad + \frac{t_0^2 (e^{-2\gamma T} - e^{-2\gamma t_0})^2 \sin^2(\omega_0 t_0) \cos^2(\omega_0 t_0)}{1 - e^{-2\gamma T} \sin^2(\omega_0 t_0) - e^{-2\gamma t_0} \cos^2(\omega_0 t_0)}. \end{aligned}$$

Appendix F: Spontaneous emission

For the non-controlled scheme, recall the Hamiltonian of this example is $H = \frac{1}{2} \omega_0 \sigma_3$ and the master equation for the spontaneous emission is

$$\begin{aligned} \partial_t \rho(t) &= -i[H, \rho] + \gamma_+ \left[\sigma_+ \rho(t) \sigma_- - \frac{1}{2} \{ \sigma_- \sigma_+, \rho(t) \} \right] \\ &\quad + \gamma_- \left[\sigma_- \rho(t) \sigma_+ - \frac{1}{2} \{ \sigma_+ \sigma_-, \rho(t) \} \right], \quad (\text{F1}) \end{aligned}$$

The solution for the master equation is

$$\rho_{00}(t) = e^{-(\gamma_+ + \gamma_-)t} \rho_{00}(0) + \frac{\gamma_+}{\gamma_+ + \gamma_-} \left[1 - e^{-(\gamma_+ + \gamma_-)t} \right],$$

$$\rho_{01}(t) = e^{-i\omega_0 t - \frac{1}{2}(\gamma_+ + \gamma_-)t} \rho_{01}(0).$$

In the Bloch representation, we have

$$\begin{aligned} r_1(t) &= e^{-\frac{1}{2}(\gamma_+ + \gamma_-)t} [\cos(\omega_0 t) r_1(0) - \sin(\omega_0 t) r_2(0)], \\ r_2(t) &= e^{-\frac{1}{2}(\gamma_+ + \gamma_-)t} [\cos(\omega_0 t) r_2(0) + \sin(\omega_0 t) r_1(0)], \\ r_3(t) &= \frac{\gamma_+ - \gamma_-}{\gamma_+ + \gamma_-} \left[1 - e^{-(\gamma_+ + \gamma_-)t} \right] + e^{-(\gamma_+ + \gamma_-)t} r_3(0). \end{aligned}$$

For the initial state $|+\rangle$, the evolved Bloch vector reads

$$r_1(t) = e^{-\frac{1}{2}(\gamma_+ + \gamma_-)t} \cos(\omega_0 t), \quad (\text{F2})$$

$$r_2(t) = e^{-\frac{1}{2}(\gamma_+ + \gamma_-)t} \sin(\omega_0 t), \quad (\text{F3})$$

$$r_3(t) = \frac{\gamma_+ - \gamma_-}{\gamma_+ + \gamma_-} \left[1 - e^{-(\gamma_+ + \gamma_-)t} \right]. \quad (\text{F4})$$

From these expressions, we have $|\partial_{\omega_0} \vec{r}(T)|^2 = e^{-(\gamma_+ + \gamma_-)T} T^2$ and $\vec{r}(T) \cdot \partial_{\omega_0} \vec{r}(T) = 0$, thus, the QFI at target time for non-controlled scheme is

$$F = e^{-(\gamma_+ + \gamma_-)T} T^2. \quad (\text{F5})$$

Next we perform a single rotation strategy as an intuitive mechanism for the effect of control: the Bloch vector is rotated by the control to $x - y$ plane along the y axis at time t_0 . Before the rotation, the Bloch vector is

$$r_1(t_0) = e^{-\frac{1}{2}(\gamma_+ + \gamma_-)t_0} \cos(\omega_0 t_0), \quad (\text{F6})$$

$$r_2(t_0) = e^{-\frac{1}{2}(\gamma_+ + \gamma_-)t_0} \sin(\omega_0 t_0), \quad (\text{F7})$$

$$r_3(t_0) = \frac{\gamma_+ - \gamma_-}{\gamma_+ + \gamma_-} \left[1 - e^{-(\gamma_+ + \gamma_-)t_0} \right]. \quad (\text{F8})$$

In the following we assume $\gamma_+ = 0$ and $\gamma_- = \gamma$, above expressions then reduce to

$$r_1(t_0) = e^{-\gamma t_0} \cos(\omega_0 t_0), \quad (\text{F9})$$

$$r_2(t_0) = e^{-\gamma t_0} \sin(\omega_0 t_0), \quad (\text{F10})$$

$$r_3(t_0) = -1 + e^{-\gamma t_0}. \quad (\text{F11})$$

Now we perform the rotation $R_{y,1}$ in the form below

$$\left(\begin{array}{cc} \frac{r_1(t_0)|_{\omega_0=\bar{\omega}_0}}{\sqrt{r_1^2(t_0)|_{\omega_0=\bar{\omega}_0} + r_3^2(t_0)|_{\omega_0=\bar{\omega}_0}}} & 0 \\ 0 & 1 \\ -\frac{r_3(t_0)|_{\omega_0=\bar{\omega}_0}}{\sqrt{r_1^2(t_0)|_{\omega_0=\bar{\omega}_0} + r_3^2(t_0)|_{\omega_0=\bar{\omega}_0}}} & 0 \end{array} \right) \begin{array}{c} \frac{r_3(t_0)|_{\omega_0=\bar{\omega}_0}}{\sqrt{r_1^2(t_0)|_{\omega_0=\bar{\omega}_0} + r_3^2(t_0)|_{\omega_0=\bar{\omega}_0}}} \\ 0 \\ \frac{r_1(t_0)|_{\omega_0=\bar{\omega}_0}}{\sqrt{r_1^2(t_0)|_{\omega_0=\bar{\omega}_0} + r_3^2(t_0)|_{\omega_0=\bar{\omega}_0}}} \end{array},$$

where $\bar{\omega}_0$ is the true value of ω_0 . After the rotation, we have

$$R_{y,1} \vec{r}(t_0) = \left(\begin{array}{c} \frac{r_1(t_0)|_{\omega_0=\bar{\omega}_0} r_1(t_0) + r_3(t_0)|_{\omega_0=\bar{\omega}_0} r_3(t_0)}{\sqrt{r_1^2(t_0)|_{\omega_0=\bar{\omega}_0} + r_3^2(t_0)|_{\omega_0=\bar{\omega}_0}}} \\ r_2(t_0) \\ \frac{-r_3(t_0)|_{\omega_0=\bar{\omega}_0} r_1(t_0) + r_1(t_0)|_{\omega_0=\bar{\omega}_0} r_3(t_0)}{\sqrt{r_1^2(t_0)|_{\omega_0=\bar{\omega}_0} + r_3^2(t_0)|_{\omega_0=\bar{\omega}_0}}} \end{array} \right). \quad (\text{F12})$$

Then the Bloch vector at target time T reads

$$r_1(T) = e^{-\frac{1}{2}\gamma(T-t_0)} \left\{ \cos[\omega_0(T-t_0)] \frac{r_1(t_0)|_{\omega_0=\bar{\omega}_0} r_1(t_0) + r_3(t_0)|_{\omega_0=\bar{\omega}_0} r_3(t_0)}{\sqrt{r_1^2(t_0)|_{\omega_0=\bar{\omega}_0} + r_3^2(t_0)|_{\omega_0=\bar{\omega}_0}}} - \sin[\omega_0(T-t_0)] r_2(t_0) \right\}, \quad (\text{F13})$$

$$r_2(T) = e^{-\frac{1}{2}\gamma(T-t_0)} \left\{ \cos[\omega_0(T-t_0)] r_2(t_0) + \sin[\omega_0(T-t_0)] \frac{r_1(t_0)|_{\omega_0=\bar{\omega}_0} r_1(t_0) + r_3(t_0)|_{\omega_0=\bar{\omega}_0} r_3(t_0)}{\sqrt{r_1^2(t_0)|_{\omega_0=\bar{\omega}_0} + r_3^2(t_0)|_{\omega_0=\bar{\omega}_0}}} \right\}, \quad (\text{F14})$$

$$r_3(T) = -1 + e^{-\gamma(T-t_0)} + e^{-\gamma(T-t_0)} \frac{-r_3(t_0)|_{\omega_0=\bar{\omega}_0} r_1(t_0) + r_1(t_0)|_{\omega_0=\bar{\omega}_0} r_3(t_0)}{\sqrt{r_1^2(t_0)|_{\omega_0=\bar{\omega}_0} + r_3^2(t_0)|_{\omega_0=\bar{\omega}_0}}}. \quad (\text{F15})$$

At the point $\omega_0 = \bar{\omega}_0$, the Bloch vector is

$$r_1(T)|_{\omega_0=\bar{\omega}_0} = e^{-\frac{1}{2}\gamma T} \left\{ \cos[\bar{\omega}_0(T-t_0)] \sqrt{\cos^2(\bar{\omega}_0 t_0) + e^{\gamma t_0} - 2 + e^{-\gamma t_0}} - \sin[\bar{\omega}_0(T-t_0)] \sin(\bar{\omega}_0 t_0) \right\}, \quad (\text{F16})$$

$$r_2(T)|_{\omega_0=\bar{\omega}_0} = e^{-\frac{1}{2}\gamma T} \left\{ \cos[\bar{\omega}_0(T-t_0)] \sin(\bar{\omega}_0 t_0) + \sin[\bar{\omega}_0(T-t_0)] \sqrt{\cos^2(\bar{\omega}_0 t_0) + e^{\gamma t_0} - 2 + e^{-\gamma t_0}} \right\}, \quad (\text{F17})$$

$$r_3(T)|_{\omega_0=\bar{\omega}_0} = -1 + e^{-\gamma(T-t_0)}. \quad (\text{F18})$$

The derivative of Bloch vector at $\omega_0 = \bar{\omega}_0$ is

$$\begin{aligned} [\partial_{\omega_0} r_1(T)]|_{\omega_0=\bar{\omega}_0} &= e^{-\frac{1}{2}\gamma T} \left\{ -(T-t_0) \sin[\bar{\omega}_0(T-t_0)] \sqrt{\cos^2(\bar{\omega}_0 t_0) + e^{\gamma t_0} - 2 + e^{-\gamma t_0}} + t_0 \sin[\bar{\omega}_0(2t_0-T)] \right. \\ &\quad \left. - \cos[\bar{\omega}_0(T-t_0)] \sin(\bar{\omega}_0 t_0) \left(\frac{t_0 \cos(\bar{\omega}_0 t_0)}{\sqrt{\cos^2(\bar{\omega}_0 t_0) + e^{\gamma t_0} - 2 + e^{-\gamma t_0}}} - T \right) \right\}, \end{aligned} \quad (\text{F19})$$

and

$$\begin{aligned} [\partial_{\omega_0} r_2(T)]|_{\omega_0=\bar{\omega}_0} &= e^{-\frac{1}{2}\gamma T} \left\{ (T-t_0) \cos[\bar{\omega}_0(T-t_0)] \sqrt{\cos^2(\bar{\omega}_0 t_0) + e^{\gamma t_0} - 2 + e^{-\gamma t_0}} + t_0 \cos[\bar{\omega}_0(2t_0-T)] \right. \\ &\quad \left. - \sin[\bar{\omega}_0(T-t_0)] \sin(\bar{\omega}_0 t_0) \left(\frac{t_0 \cos(\bar{\omega}_0 t_0)}{\sqrt{\cos^2(\bar{\omega}_0 t_0) + e^{\gamma t_0} - 2 + e^{-\gamma t_0}}} + T \right) \right\}, \end{aligned} \quad (\text{F20})$$

and

$$[\partial_{\omega_0} r_3(T)]|_{\omega_0=\bar{\omega}_0} = \frac{[e^{-\gamma T} - e^{-\gamma(T-t_0)}] t_0 \sin(\bar{\omega}_0 t_0)}{\sqrt{\cos^2(\bar{\omega}_0 t_0) + e^{\gamma t_0} - 2 + e^{-\gamma t_0}}}. \quad (\text{F21})$$

The QFI can then be obtained via Eq. (E4).

-
- [1] V. Giovannetti, S. Lloyd and L. Maccone, Advances in quantum metrology, *Nature Photonics* **5**, 222-229 (2011).
[2] V. Giovannetti, S. Lloyd, and L. Maccone, Quantum-enhanced measurements: Beating the standard quantum limit. *Science* **306**, 1330-1336 (2004).
[3] C. M. Caves, Quantum-mechanical noise in an interferometer, *Phys. Rev. D* **23**, 1693-1708 (1981).
[4] P. M. Anisimov, G. M. Raterman, A. Chiruvelli, W. N. Plick, S. D. Huver, H. Lee and J. P. Dowling, Quantum Metrology with Two-Mode Squeezed Vacuum: Parity Detection Beats the Heisenberg Limit, *Phys. Rev. Lett.* **104**, 103602 (2010).
[5] S. L. Braunstein, Quantum limits on precision measurements of phase, *Phys. Rev. Lett.* **69**, 3598-3601 (1992).
[6] A. Fujiwara and H. Imai, A fibre bundle over manifolds of quantum channels and its application to quantum statistics, *J. Phys. A* **41**, 255304 (2008).
[7] M. G. A. Paris, Quantum estimation for quantum technology, *Int. J. Quant. Inf.* **7** 125 (2009).
[8] B. M. Escher, R. L. de Matos Filho and L. Davidovich, General framework for estimating the ultimate precision limit in noisy quantum-enhanced metrology, *Nat. Phys.* **7**, 406-411 (2011).
[9] R. Demkowicz-Dobrzanski and L. Maccone, Using Entanglement Against Noise in Quantum Metrology, *Phys. Rev. Lett.* **113**, 250801 (2014).
[10] M. Tsang, Quantum metrology with open dynamical systems, *New J. Phys.* **15**, 073005 (2013).
[11] R. Demkowicz-Dobrzanski, J. Kolodynski and M. Guta, The elusive Heisenberg limit in quantum-enhanced metrology, *Nat. Commun.* **3**, 1063 (2012).
[12] S. Knysh, V. N. Smelyanskiy and G. A. Durkin, Scaling laws for precision in quantum interferometry and the bifurcation landscape of the optimal state, *Phys. Rev. A* **83**, 021804 (2011).
[13] S. Alipour, M. Mehboudi and A. T. Rezakhani, Quan-

- tum metrology in open systems: dissipative Cramér-Rao bound, *Phys. Rev. Lett.* **112**, 120405 (2014).
- [14] J. Joo, W. J. Munro and T. P. Spiller, Quantum metrology with entangled coherent states, *Phys. Rev. Lett.* **107**, 083601 (2011).
- [15] J. Liu, X.-X. Jing and X. Wang, Phase-matching condition for enhancement of phase sensitivity in quantum metrology, *Phys. Rev. A* **88**, 042316 (2013).
- [16] X.-M. Lu, S. Yu and C. H. Oh, Robust quantum metrological schemes based on protection of quantum Fisher information, *Nat. Commun.* **6**, 7282 (2015).
- [17] H. Yuan and C.-H. F. Fung, Optimal Feedback Scheme and Universal Time Scaling for Hamiltonian Parameter Estimation, *Phys. Rev. Lett.* **115**, 110401 (2015).
- [18] R. Chaves, J. B. Brask, M. Markiewicz, J. Kolodynski and A. Acin, Noisy Metrology beyond the Standard Quantum Limit, *Phys. Rev. Lett.* **111**, 120401 (2013).
- [19] L. A. Correa, M. Mehboudi, G. Adesso and A. Sanpera, Individual Quantum Probes for Optimal Thermometry, *Phys. Rev. Lett.* **114**, 220405 (2015).
- [20] G. Toth and I. Apellaniz, Quantum metrology from a quantum information science perspective, *J. Phys. A* **47**, 424006 (2014).
- [21] L. Pezze and Augusto Smerzi, Mach-Zehnder Interferometry at the Heisenberg Limit with Coherent and Squeezed-Vacuum Light, *Phys. Rev. Lett.* **100**, 073601 (2008).
- [22] D. W. Berry, M. Tsang, M. J. W. Hall, and H. M. Wiseman, Quantum Bell-Ziv-Zakai Bounds and Heisenberg Limits for Waveform Estimation, *Phys. Rev. X* **5**, 031018 (2015).
- [23] A. A. Berni, T. Gehring, B. M. Nielsen, V. Handchen, M. G. A. Paris and U. L. Andersen, Ab initio quantum-enhanced optical phase estimation using real-time feedback control, *Nature Photonics* **9**, 577-581 (2015).
- [24] T. Baumgratz and A. Datta, Quantum Enhanced Estimation of a Multidimensional Field, *Phys. Rev. Lett.* **116**, 030801 (2016).
- [25] H. Yuan, Sequential feedback scheme outperforms the parallel scheme for Hamiltonian parameter estimation, *Phys. Rev. Lett.* **117**, 160801 (2016).
- [26] C. W. Helstrom, *Quantum Detection and Estimation Theory* (Academic, New York, 1976).
- [27] A. S. Holevo, *Probabilistic and Statistical Aspects of Quantum Theory* (North-Holland, Amsterdam, 1982).
- [28] S. L. Braunstein and C. M. Caves, Statistical distance and the geometry of quantum states, *Phys. Rev. Lett.* **72**, 3439-3443 (1994).
- [29] S. L. Braunstein, C. M. Caves and G. J. Milburn, Generalized uncertainty relations: Theory, examples, and Lorentz invariance, *Ann. of Phys.* **247**, 135-173 (1996).
- [30] V. Giovannetti, S. Lloyd and L. Maccone, Quantum Metrology, *Phys. Rev. Lett.* **96**, 010401 (2006).
- [31] Q.-S. Tan, Y. Huang, X. Yin, L.-M. Kuang and X. Wang, Enhancement of parameter-estimation precision in noisy systems by dynamical decoupling pulses, *Phys. Rev. A* **87**, 032102 (2013).
- [32] J. E. Lang, R. B. Liu and T. S. Monteiro, Dynamical-Decoupling-Based Quantum Sensing: Floquet Spectroscopy, *Phys. Rev. X* **5**, 041016 (2015).
- [33] N. Zhao and Z.-q. Yin, Room-temperature ultrasensitive mass spectrometer via dynamical decoupling, *Phys. Rev. A* **90**, 042118 (2014).
- [34] Q. Zheng, L. Ge, Y. Yao and Q.-j. Zhi, Enhancing parameter precision of optimal quantum estimation by direct quantum feedback, *Phys. Rev. A* **91**, 033805 (2015).
- [35] P. Sekatski, M. Skotiniotis and W. Dur, Dynamical decoupling leads to improved scaling in noisy quantum metrology, *New J. Phys.* **18**, 073034 (2016).
- [36] P. Sekatski, M. Skotiniotis, J. Kolodynski and W. Dur, Quantum metrology with full and fast quantum control, arXiv: 1603.08944.
- [37] E. M. Kessler, I. Lovchinsky, A. O. Sushkov and M. D. Lukin, Quantum Error Correction for Metrology, *Phys. Rev. Lett.* **112**, 150802 (2014).
- [38] W. Dur, M. Skotiniotis, F. Frowis and B. Kraus, Improved Quantum Metrology Using Quantum Error Correction, *Phys. Rev. Lett.* **112**, 080801 (2014).
- [39] G. Arrad, Y. Vinkler, D. Aharonov and A. Retzker, Increasing Sensing Resolution with Error Correction, *Phys. Rev. Lett.* **112**, 150801 (2014).
- [40] R. Ozeri, Heisenberg limited metrology using Quantum Error-Correction Codes, arXiv: 1310.3432.
- [41] R. Nichols, T. R. Bromley, L. A. Correa and G. Adesso, Practical quantum metrology in noisy environments, *Phys. Rev. A* **94**, 042101 (2016).
- [42] N. Khaneja, T. Reiss, C. Hehlet, T. Schulte-Herbruggen and S. J. Glaser, Optimal control of coupled spin dynamics: design of NMR pulse sequences by gradient ascent algorithms, *J. Magn. Res.* **172**, 296-305 (2005).
- [43] H.-P. Breuer and F. Petruccione, *The Theory of Open Quantum Systems* (Oxford University Press, Oxford, 2007).
- [44] R. R. Ernst, G. Bodenhausen and A. Wokaun, *Principles of Nuclear Magnetic Resonance in One and Two Dimensions* (Clarendon Press, Oxford, 1987).
- [45] S. E. Sklarz, D. J. Tannor, and N. Khaneja, Optimal control of quantum dissipative dynamics: Analytic solution for cooling the three-level Λ system, *Phys. Rev. A* **69**, 053408 (2004).
- [46] D. J. Tannor and A. Bartana, On the Interplay of Control Fields and Spontaneous Emission in Laser Cooling, *J. Phys. Chem. A* **103**, 10359-10363 (1999).
- [47] Another way to understand this assumption is to take it as the limit of discrete pulses, where the evolution with the controls within δt is $e^{(\mathcal{L}+\mathcal{H}_c)\delta t}$, here \mathcal{L} is the original operator and \mathcal{H}_c comes from the added control, using the Trotter formula this can be thought of as the original evolution interspersed by fast controls, i.e., $e^{(\mathcal{L}+\mathcal{H}_c)\delta t} \approx (e^{\mathcal{L}\delta t/n} e^{\mathcal{H}_c\delta t/n})^n$. The continuous controls can thus be taken as the limit of the discrete pulses where the noises are not affected as long as the controls can be made fast enough (fast controls mean that the discrete pulses $e^{\mathcal{H}_c\delta t/n}$ can be realized by a stronger control field with much less time so the evolution of \mathcal{L} can be neglected).
- [48] S. Machnes, U. Sander, S. J. Glaser, P. de Fouquieres, A. Gruslys, S. Schirmer and T. Schulte-Herbruggen, Comparing, optimizing, and benchmarking quantum-control algorithms in a unifying programming framework, *Phys. Rev. A* **84**, 022305 (2011).
- [49] L. Childress, M. V. Gurudev Dutt, J. M. Taylor, A. S. Zibrov, F. Jelezko, J. Wrachtrup, P. R. Hemmer and M. D. Lukin, Coherent Dynamics of Coupled Electron and Nuclear Spin Qubits in Diamond, *Science* **314**, 281-285 (2006).
- [50] M. V. Gurudev Dutt, L. Childress, L. Jiang, E. Togan, J.

- Maze, F. Jelezko, A. S. Zibrov, P. R. Hemmer and M. D. Lukin, Quantum Register Based on Individual Electronic and Nuclear Spin Qubits in Diamond, *Science* **316**, 1312-1316 (2007).
- [51] W. Zhong, Z. Sun, J. Ma, X. Wang and F. Nori, Fisher information under decoherence in Bloch representation, *Phys. Rev. A* **87**, 022337 (2013).
- [52] G. Rancan, T. T. Nguyen and S. J. Glaser, Gradient ascent pulse engineering for rapid exchange saturation transfer, *J. Magn. Res.* **252**, 1-9 (2015).
- [53] S. S. Kocher, T. Heydenreich, S.J. Glaser, Visualization and analysis of modulated pulses in magnetic resonance by joint time-frequency representations, *J. Magn. Res.* **249**, 63-71 (2014).
- [54] van I. Maximov, Z. Tosner and Niels Chr. Nielsen, Optimal control design of NMR and dynamic nuclear polarization experiments using monotonically convergent algorithms, *J. Chem. Phys.* **128**, 184505 (2008).
- [55] P. E. Spindler, Y. Zhang, B. Endeward, N. Gershernzon, T. E. Skinner, S. J. Glaser and T. F. Prisner, Shaped optimal control pulses for increased excitation bandwidth in EPR, *J. Magn. Res.* **218**, 49-58 (2012).
- [56] C. A. Ryan, C. Negrevergne, M. Laforest, E. Knill and R. Laflamme, Liquid-state nuclear magnetic resonance as a testbed for developing quantum control methods, *Phys. Rev. A* **78**, 012328 (2008).
- [57] B. Bartels, Smooth Optimal Control of Coherent Quantum Dynamics, Ph.D. Dissertation, School of Soft Matter, Freiburg Institute for Advanced Studies, Albert-Ludwigs-Universität Freiburg (2015).
- [58] J.-S. Li, J. Ruthsa, T.-Y. Yub, H. Arthanarib and G. Wagnerb, Optimal pulse design in quantum control: A unified computational method, *Proceedings of the National Academy of Sciences* **108** (5), 1879-1884 (2011).
- [59] J. Scheuer, X. Kong, R. S. Said, J. Chen, A. Kurz, L. Marseglia, J. Du, P. R. Hemmer, S. Montangero, T. Calarco, B. Naydenov, and F. Jelezko, Precise qubit control beyond the rotating wave approximation, *New J. Phys.* **16**, 093022 (2014).
- [60] F. Dolde, V. Bergholm, Y. Wang, I. Jakobi, B. Naydenov, S. Pezzagna, J. Meijer, F. Jelezko, P. Neumann, T. Schulte-Herbruggen, J. Biamonte, and J. Wrachtrup, High-fidelity spin entanglement using optimal control, *Nat. Commun.* **5**, 3371 (2014).
- [61] X. Rong, J. Geng, Z. Wang, Q. Zhang, C. Ju, F. Shi, C.-K. Duan and J. Du, Implementation of Dynamically Corrected Gates on a Single Electron Spin in Diamond, *Phys. Rev. Lett.* **112**, 050503 (2014)
- [62] R. Bucker, T. Berrada, S. van Frank, J.-F. Schaff, T. Schumm, J. Schmiedmayer, G. Jager, J. Grond, and U. Hohenester, Vibrational state inversion of a Bose-Einstein condensate: optimal control and state tomography, *J. Phys. B* **46**, 104012 (2013).
- [63] D. M. Reich, N. Katz and C. P. Koch, Exploiting Non-Markovianity for Quantum Control. *Sci. Rep.* **5**, 12430 (2015).
- [64] P. Rebentrost, I. Serban, T. Schulte-Herbruggen and F. K. Wilhelm, Optimal Control of a Qubit Coupled to a Non-Markovian Environment, *Phys. Rev. Lett.* **102**, 090401 (2009).
- [65] R. Schmidt, A. Negretti, J. Ankerhold, T. Calarco and J. T. Stockburger, Optimal Control of Open Quantum Systems: Cooperative Effects of Driving and Dissipation, *Phys. Rev. Lett.* **107**, 130404 (2011).
- [66] G. Dridi, M. Lapert, J. Salomon, S. J. Glaser and D. Sugny, Discrete-valued-pulse optimal control algorithms: Application to spin systems, *Phys. Rev. A* **92**, 043417 (2015).
- [67] S. Machnes, U. Sander, S. J. Glaser, P. de Fouquieres, A. Gruslys, S. Schirmer and T. Schulte-Herbruggen, Comparing, optimizing, and benchmarking quantum-control algorithms in a unifying programming framework, *Phys. Rev. A* **84**, 022305 (2011).
- [68] C. P. Koch, Controlling open quantum systems: tools, achievements, and limitations, *J. Phys.: Condens. Matter* **28** 213001 (2016).